EJN fens EUROPEAN JOURNAL OF NEUROSCIENCE

European Journal of Neuroscience, Vol. 36, pp. 2801–2811, 2012 doi:10.1111/j.1460-9568.2012.08195.x

NEUROSYSTEMS

Visual capabilities and cortical maps in BALB/c mice

Naira Yeritsyan,[1,*] Konrad Lehmann,[2,*] Oliver Puk,[3] Jochen Graw[3] and Siegrid Löwel[2,†]
[1]Leibniz-Institut für Neurobiologie, Magdeburg, Germany
[2]Institut für Allgemeine Zoologie und Tierphysiologie, Friedrich-Schiller-Universität Jena, Erbertstr. 1, D-07743 Jena, Germany
[3]Helmholtz Zentrum München, Institute of Developmental Genetics, German Research Centre for Environmental Health, Neuherberg, Germany

Keywords: albino mice, optical imaging, optometry, sensory learning, visual cortex

Abstract

By combining behavioural analyses with intrinsic signal optical imaging, we analysed visual performance and visual cortical activity in the albino mouse strain BALB/c, which is increasingly being used as an animal model of neuropsychological disorders. Visual acuity, as measured by a virtual-reality optomotor system, was 0.12 cycles per degree (cyc/deg) in BALB/c mice and 0.39 cyc/deg in pigmented C57BL/6 mice. Surprisingly, BALB/c mice showed reflexive head movements against the direction of the rotating stimulus. Contrast sensitivity was significantly lower in BALB/c mice (45% contrast at 0.064 cyc/deg) than in C57BL/6 mice (6% contrast). In the visual water task, visual acuity was 0.3 cyc/deg in BALB/c mice and 0.59 cyc/deg in C57BL/6 mice. Thus, the visual performance of BALB/c mice was significantly impaired in both behavioural tests – visual acuity was $\sim$ 0.3 cyc/deg lower than in C57BL/6 mice, and contrast sensitivity was reduced by a factor of $\sim$ 8. In BALB/c mice, visual cortical maps induced by stimulation of the contralateral eye were normal in both activation strength and retinotopic map quality. In contrast, maps induced by ipsilateral eye stimulation differed significantly between the strains – activity in a region representing 15° to 19° elevation in the visual field was significantly weaker in BALB/c mice than in C57BL/6 mice. Taken together, our observations show that BALB/c mice, like the albino animals of other species, have a significantly lower visual performance than C57BL/6 mice and a modified cortical representation of the ipsilateral eye that may impair stereopsis. Thus, our results caution against disregarding vision as a confounding factor in behavioural tests of neuropsychological disorders.

Introduction

As many behavioural tests that are used to characterize the effects of genetic manipulations in mice rely on visual information, the study of visual capabilities in inbred strains is of growing importance. Commonly used in immunological and cardiovascular studies, mice of the BALB/c strain have recently become a subject of wide interest in electrophysiological and behavioural research (Holthoff *et al.*, 2004; Lepicard *et al.*, 2006; Brodkin, 2007; Kohara *et al.*, 2007; Moy *et al.*, 2008). Recently, BALB/c has been suggested as a candidate strain with which to model core symptoms of autism, owing to reduced exploration, anxiety-like behaviour, neophob'ia, and low social approach (Sankoorikal *et al.*, 2006; Brodkin, 2007; Moy *et al.*, 2008). However, the motor and cognitive defects in behavioural studies (Klapdor & van der Staay, 1996; McFadyen *et al.*, 2003; Brodkin, 2007) can be confounded by poor vision, one of the key syndromes of oculocutaneous albinism in all mammalian species. Among rodents, a visual acuity of only about half the value measured in pigmented strains was found in three albino rat strains, by use of a visual discrimination task, the so-called visual water task (VWT) (Prusky *et al.*, 2002). However, exact data on the visual capabilities of BALB/c mice are still lacking, because, in previous studies using the VWT, these animals failed to reach criterion even with the lowest spatial frequencies used (Wong & Brown, 2006), and reflexive head tracking to horizontally rotating bars could not be observed (Puk *et al.*, 2008).

In the present study, we used two different behavioural tests – a virtual-reality optomotor system and the VWT – to investigate the visual capabilities of BALB/c mice. By carefully observing the mice in the virtual-reality optomotor system, we detected a reflexive tracking response against the direction of the moving visual stimuli that we used to determine both visual acuity and contrast thresholds. Furthermore, we managed to train BALB/c mice in a visual discrimination task by reducing the number of trials per day and allowing for longer training times, so that we could additionally determine their perceptual visual acuity.

Correspondences: Siegrid Löwel, †Present address below.
E-mail: sloewel@gwdg.de
Konrad Lehmann, as above.
E-mail: konrad.lehmann@uni-jena.de

*N.Y. and K.L. contributed equally to this work.

†*Present address*: Systems Neuroscience, Bernstein Focus Neurotechnology (BFNT) and Johann-Friedrich-Blumenbach Institut für Zoologie und Anthropologie, Universität Göttingen, Von-Siebold-Str. 4, D-37075 Göttingen, Germany.

Received 6 March 2012, revised 23 May 2012, accepted 23 May 2012

Whether the poor vision of albino mammals is related to abnormalities in the visual cortex is also mostly unknown. One study using only two BALB/c animals found that visual cortical activation was much lower in BALB/c mice than in C57BL/6 mice (Heimel *et al.*, 2007). In albinos of the C57BL/6 strain, visual cortical retinotopy was apparently normal (Dräger & Olsen, 1980). However, an exceedingly weak ipsilateral projection to the visual cortex seems to be a common feature in albino rodents (Lund, 1965; Dräger, 1974; Dräger & Olsen, 1980), and is probably the cause of the very high contralateral dominance in the BALB/c visual cortex observed by optical imaging (Heimel *et al.*, 2007). Whether the ipsilateral projection is otherwise normal is not yet known. To address this question, we used optical imaging of intrinsic signals (Kalatsky & Stryker, 2003; Lehmann & Löwel, 2008) to visualize cortical activity maps induced by visual stimulation of both the ipsilateral and contralateral eye in BALB/c mice.

Materials and methods

Subjects

Forty BALB/c and 26 C57BL/6 mice between postnatal day (P)88 and P108 were used in this study. The mice were raised in standard cages on a 12-h light/dark cycle, with food and water available *ad libitum*. Mice were reared in sibling groups. All experimental procedures were performed according to the German Law on the Protection of Animals and the corresponding European Communities Council Directive of 24 November 1986 (86/609/EEC), and were approved by the local government under the registration number 02-015/06.

Visual acuity and contrast sensitivity

Virtual optomotor system

Visual acuity was assessed with a virtual-reality optomotor system (Prusky *et al.*, 2004). Briefly, freely moving animals are exposed to moving sine wave gratings of various spatial frequencies and contrasts, and will reflexively track the gratings by head movements as long as they can see the gratings. In each eye, the reflex is only triggered by gratings moving in the temporo-nasal direction, which allows measurement of the thresholds in both eyes separately. Spatial frequency at full contrast was increased until no tracking could be observed. Contrast sensitivity was measured at six different spatial frequencies [0.031, 0.064, 0.092, 0.103, 0.192 and 0.272 cycles per degree (cyc/deg)] by decreasing contrast until the threshold of tracking was determined. The behavioural threshold at a spatial frequency was calculated as a Michelson contrast from the screen's luminances ([maximum − minimum]/[maximum + minimum]) by multiplying by 0.997 (black mean, 0.22 cd/m^2; white mean, 152.13 cd/m^2). The contrast sensitivity (the reciprocal of the threshold) was then plotted against spatial frequency on a log–log graph – 25% contrast thus corresponds to 4.01 contrast sensitivity.

VWT

As a second method to assess visual acuity, we used the VWT, a visual discrimination task that is based on reinforcement learning (Prusky *et al.*, 2000; Prusky & Douglas, 2004).

For this task, animals are initially trained to distinguish a low spatial frequency vertical grating (0.086 cyc/deg) from equiluminant grey, and their ability to recognize higher spatial frequencies is then tested. The apparatus consists of a trapezoidal-shaped pool with two monitors placed side by side at one end. A midline divider is extended from the wide end into the pool, creating a maze with a stem and two arms. The length of the divider sets the choice point between the homogeneous grey and the effective spatial frequency. An escape platform that is invisible to the animals is placed below the monitor on which the grating is projected. The position of the grating and the platform is alternated in a pseudorandom sequence over the training and test trials. When 90% accuracy is achieved, the discrimination threshold is determined by increasing the spatial frequency of the grating until performance falls below 70% accuracy. The highest spatial frequency at which 70% accuracy is achieved is taken as the maximum visual acuity. The control C57BL/6 mice were trained and tested in groups of four in sessions of seven to 15 interleaved trials. As the state of albino animals had already worsened after the fifth swimming trial – their floating time increased, they looked exhausted, and they gave up grooming attempts to dry out in their holding cage – the number of training and testing trials for BALB/c mice was reduced to five trials per session. Although this manoeuvre prolonged the training and testing procedures, it allowed completion of the task for BALB/c mice with the determination of visual acuity thresholds. Between trials, all mice were allowed to dry and warm up in the holding cage. No more than two sessions separated by at least 1 h were run in a single day. The entire task was performed with the room lights off.

Optical imaging of intrinsic signals

Surgical preparation for optical imaging

We always recorded visual cortical activity in the left brain hemisphere. After initial anaesthesia with 2% halothane in a 1 : 1 O_2/N_2O mixture, non-deprived and monocularly deprived animals received an intraperitoneal injection of 50 mg/kg pentobarbital, supplemented with intramuscular chlorprothixene (0.2 mg per mouse), subcutaneous atropine (0.3 mg per mouse), and subcutaneous dexamethasone (0.2 mg per mouse). Lidocaine (2% xylocaine jelly) was applied locally to all cutaneous incisions. After tracheotomy, a tracheal tube was inserted and fixed by a ligature. Mice were placed in a stereotaxic apparatus. Body temperature was maintained at 37 °C, and the electrocardiogram was monitored throughout the experiment. The constant level of anaesthesia was additionally controlled by checking the spinal reflexes, and kept stable with 0.6–0.8% halothane in 1 : 1 O_2/N_2O delivered through the tracheal tube. A craniotomy was made over the left hemisphere. The exposed area was covered with agarose (2.5% in saline) and a glass coverslip. In six BALB/c mice, the imaging was performed through the intact skull to exclude the possible effects of craniotomy on imaging values (see below). In these cases, agarose and a glass coverslip were placed over the imaged area directly onto the skull. Data obtained with the two methods were not significantly different ($P > 0.15$ for all analyzed values, *t*-test), and were therefore pooled.

Recording visual cortical responses by optical imaging

Mouse visual cortex responses were recorded with the imaging method developed by Kalatsky & Stryker (2003) (see also Lehmann & Löwel, 2008). Briefly, optical images of cortical intrinsic signals were obtained with a Dalsa 1M30 CCD camera (Dalsa, Waterloo, ON, Canada) controlled by custom software. Using a 135 mm × 50-mm tandem lens (Nikon, Melville, NY, USA) configuration, we imaged a cortical area of 4.6 × 4.6 mm^2. The surface vascular pattern and intrinsic signal images were visualized with illumination wavelengths set by a green (550 ± 5 nm) or a red (610 ± 5 nm) interference filter, respectively. After acquisition of the surface vascular pattern, the

focus was lowered 600 μm into the cortex for intrinsic signal imaging. Frames were acquired at a rate of 30 Hz, temporally binned to 7.5 Hz, and stored as 512 × 512-pixel images after spatial binning of the camera image.

A high refresh rate CRT monitor (Dell D2128-TCO, 800 × 600 at 120 Hz) was used to display the visual stimuli – a horizontal bar drifted up and down to reveal elevation maps, and a vertical bar drifted left and right to reveal azimuth maps. Drifting horizontal or vertical bars were generated with a Matrox G450 board (Matrox Graphics, Dorval, QC, Canada), controlled by custom software. The drifting bars were 2° wide, corresponding to a spatial frequency of 0.25 cyc/deg. The distance between two bars was 80°, and they were presented at a temporal frequency of 0.125 Hz.

To quantify maximum response strength (visual cortical activity) and the quality of retinotopic maps, the monitor was placed in the right visual field of the mouse at a distance of 25 cm to optimally stimulate the right eye (contralateral to the recorded hemisphere). The visual stimuli covered 79° azimuth and 58° elevation. For the assessment of ocular dominance, the monitor was positioned in the binocular visual field of the recorded left hemisphere (−5° to +15° azimuth) in front of the mouse, and visual stimuli were presented alternately to the left and right eyes.

Data analysis

Maps were computed from the acquired frames by Fourier analysis to extract the signal at the stimulation frequency, with custom software (Kalatsky & Stryker, 2003). The phase component of the signal is used for the calculation of retinotopy, and the amplitude component represents the intensity of neuronal activation (expressed as fractional change in reflectance × 10^4).

To assess the quality of retinotopic maps, we used the calculation introduced by Cang *et al.* (2005b). Briefly, both the elevation and azimuth maps were used to select the most responsive 20 000 pixels (1.60 mm^2 of cortical space) in the visual cortex. For each of these pixels, the difference between its phase and the mean phase of its surrounding 24 pixels was calculated. For maps of high quality, the position differences are quite small, because of smooth progression. The standard deviation of the position difference was then used as an index of the quality of retinotopic maps, with small values indicating high map quality, and high values indicating low map quality [for details, see Cang *et al.* (2005b)].

Ocular dominance indices (ODIs) were calculated as described previously (Cang *et al.*, 2005a; Lehmann & Löwel, 2008). In short, activity maps were low-pass-filtered and thresholded at 30% of peak amplitude, and ocular dominance was calculated for each pixel in the binocularly responsive region as $(C - I)/(C + I)$, with C and I representing the raw magnitudes of response of each pixel to stimulation of the contralateral and ipsilateral eye, respectively, and averaged across all selected pixels. We calculated ODIs from blocks of four runs in which the averaged map for each eye had clear retinotopy and was delineated from the background. Typically, we obtained at least five ODIs per mouse; experiments with fewer than three ODIs were discarded from further analyses. The ODIs of one mouse were averaged for statistical comparisons. For comparison of the absolute amplitudes elicited by stimulation of each eye, the low-pass-filtered values were used.

We combined phase and amplitude maps of the binocular field in a tool, to analyse how much cortical activation could be elicited by the stimulus bar at a certain elevation. To this end, maps acquired by contralateral and ipsilateral eye stimulation in the binocular visual field were thresholded at 30% of peak amplitude. We then took bins of 2° elevation between −11° and 47°, in which, for each pixel, amplitude was multiplied by the pixel area (79 μm^2), and the resulting values were summed. These 'volumes' of each bin were then expressed as percentages of the total map volume. All maps of one mouse were averaged for each bin.

Histology of the eye

Eyes were fixed for 7 days in Davidson solution, and embedded in JB-4 plastic medium (Polyscience, Eppelheim, Germany), according to the manufacturer's protocol. Sectioning was performed with an ultramicrotome (OMU3; Reichert-Jung, Walldorf, Germany). Serial transverse 3-μm sections were cut with a glass knife, and stained with methylene blue and basic fuchsin. The sections were evaluated with a light microsocope (Axioplan; Carl Zeiss, Jena, Germany). Images were acquired with a scanning camera (AxioCam; Jenoptik, Jena, Germany) and imported into an image-processing program (PHOTOSHOP 10.0; Adobe, Unterschleissheim, Germany).

Optical coherence tomography (OCT)

Eye fundi and retinas were analysed with a Spectralis OCT instrument (Heidelberg Engineering, Heidelberg, Germany) modified with a 78-diopter double aspheric lens (Volk Optical, Mentor, OH, USA) fixed directly to the outlet of the device. A contact lens with a focal length of 10 mm (Roland Consult, Brandenburg, Germany) was applied to the eye of the mouse with a drop of methyl cellulose (Methocel 2%; OmniVision, Puchheim, Germany). For OCT measurements, mice were anaesthetized with 137 mg of ketamine and 6.6 mg of xylazine per kg body weight, and placed on a platform in front of the Spectralis OCT instrument such that the eye was directly facing the lens of the recording unit. Images were taken as described previously (Fischer *et al.*, 2009). Retinal thickness was routinely measured at a position close to the optic nerve head, and calculated with the provided thickness profile tool.

Statistical analysis

Contrast curves and cortical activation in the binocular field were compared by one-two and two-way ANOVA, respectively, with repeated measurements. For *post hoc* testing and inter-group comparisons, we used Student's *t*-test, Bonferroni-corrected where necessary, or the Wilcoxon rank-sum test.

Pearson correlation analysis was applied to compare the acuity values obtained in both behavioural tasks. Data are represented as means ± standard errors of the mean. The levels of significance were set as: $*P < 0.05$; $**P < 0.01$; and $***P < 0.001$.

Results

Fundus morphology and retinal structure

We stained the retinas of three BALB/c and three C57BL/6 mice with methylene blue and basic fuchsin (Fig. 1A). In all three BALB/c specimens, the retina appeared wavelike, i.e. not as smoothly concave as in C57BL/6, but with occasional convex sectors (Fig. 1A, arrows). In particular, the thickness of individual layers seemed to fluctuate along the tangential direction (Fig. 1A, arrowheads), whereas in C57BL/6 mice, the thickness of the layers was uniform or decreased consistently from the centre to the periphery. Apart from this, however, BALB/c retinas appeared normal except for the lack of pigmentation (Fig. 1B). To analyse the differences in more detail, we additionally analysed fundi and retinas of 10 BALB/c and 10

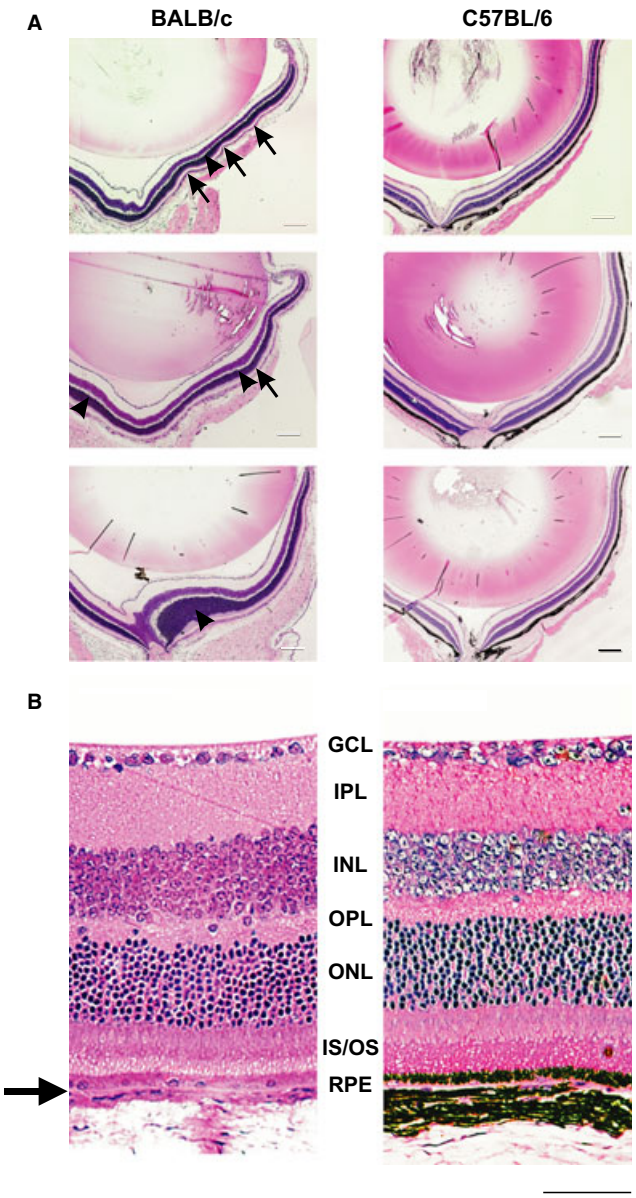

FIG. 1. Histological sections through the eyes of BALB/c mice (left) and C57BL/6 mice (right). Slices were stained with methylene blue and basic fuchsin. (A) Low-magnification view of posterior eyes in 4-month-old mice showed a wavelike retinal structure in BALB/c mice (arrows). Additionally, the thickness of individual layers could vary within small sectors (arrowheads). This was never found in sections of C57BL/6 mice. Scale bar – 200 μm. (B) Higher-magnification views of the peripheral retina of both genotypes – at the cellular level, BALB/c retinas appeared to be normally developed. GCL, ganglion cell layer; INL, inner nuclear layer; IPL, inner plexiform layer; IS/OS, inner segment/outer segment of photoreceptor layer; ONL, outer nuclear layer; OPL, outer plexiform layer; RPE, retinal pigment epithelium.

C57BL/6 mice by OCT. Whereas blood vessel patterns appeared to be normally developed in BALB/c mice as compared with C57BL/6 mice (Fig. 2A), the eye fundus background was lighter and less homogeneous in BALB/c mice. *In vivo* sections through the retina further demonstrated the lack of pigmentation in the retinal pigment epithelium of BALB/c mice. All other retinal layers were present in BALB/c mice (Fig. 2B and C); however, the distance between the retinal ganglion cell layer and the retinal pigment epithelium was slightly, but significantly, reduced in BALB/c mice as compared with C57BL/6 mice ($P < 0.001$, Wilcoxon rank-sum test; Fig. 2D).

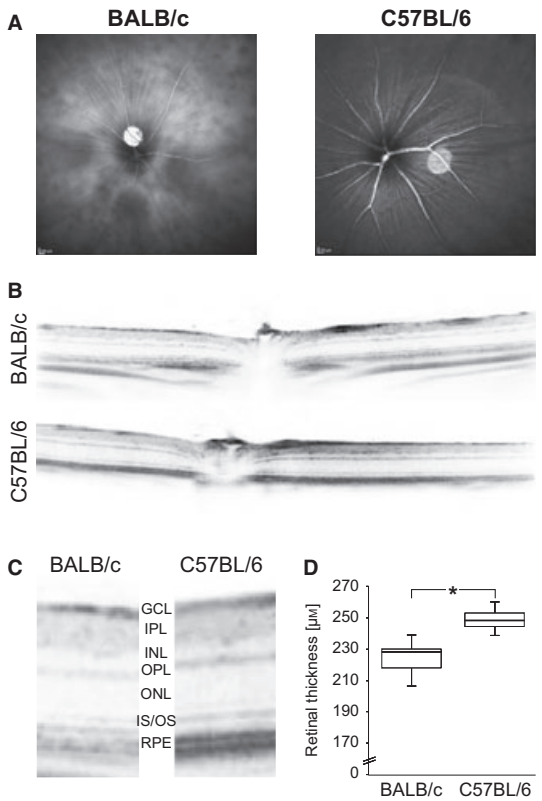

FIG. 2. OCT analysis of BALB/c and C57BL/6 mice. (A) Fundus images of 4-month-old mice indicated a lack of fundus pigmentation in BALB/c mice, resulting in a heterogeneous appearance; the vessels are regularly organized. (B) *In vivo* sections at the optic nerve level (but also in more peripheral regions of the fundus) showed regularly developed retinas in both BALB/c and C57BL/6 mice. (C) Higher magnification of the peripheral retina of both strains showed a loss of retinal epithelium pigmentation in BALB/c mice. (D) The total thickness of all retinal layers was significantly reduced in BALB/c mice as compared with C57BL/6 mice ($P < 0.001$, Wilcoxon rank-sum test). The data are shown as a box-plot indicating the median value; the bars give the highest and lowest values. GCL, ganglion cell layer; INL, inner nuclear layer; IPL, inner plexiform layer; IS/OS, inner segment/outer segment of photoreceptor layer; ONL, outer nuclear layer; OPL, outer plexiform layer; RPE, retinal pigment epithelium. *$P < 0.05$.

Visual capabilities are severely impaired in BALB/c mice

We investigated the visual performance of young adult BALB/c mice (age range, PD58–PD117; median, PD91) and C57BL/6 mice (age range, PD90–PD100; median, PD96) in both a virtual-reality optomotor system (Prusky *et al.*, 2004) and in the VWT, a task requiring visual discrimination learning (Douglas *et al.*, 2005).

Optometry

On analysis of the optomotor response to moving vertical gratings, visual acuity and contrast sensitivity values measured in the two eyes were not significantly different in either strain ($P > 0.05$, paired *t*-test), so values were averaged and means were used for all further analyses. BALB/c mice showed weak but clearly detectable head movements that were rapid in onset and decay, but surprisingly always against the direction of the rotating visual stimuli (see Movie S1). The highest spatial frequency stimulus that elicited these behavioural responses comprised moving gratings of 0.124 ± 0.01 cyc/deg ($n = 39$). Values were significantly lower than in C57BL/6 mice, which tracked these stimuli up to 0.392 ± 0.002 cyc/deg ($n = 26$, $P < 0.001$, *t*-test; Fig. 3A) and always

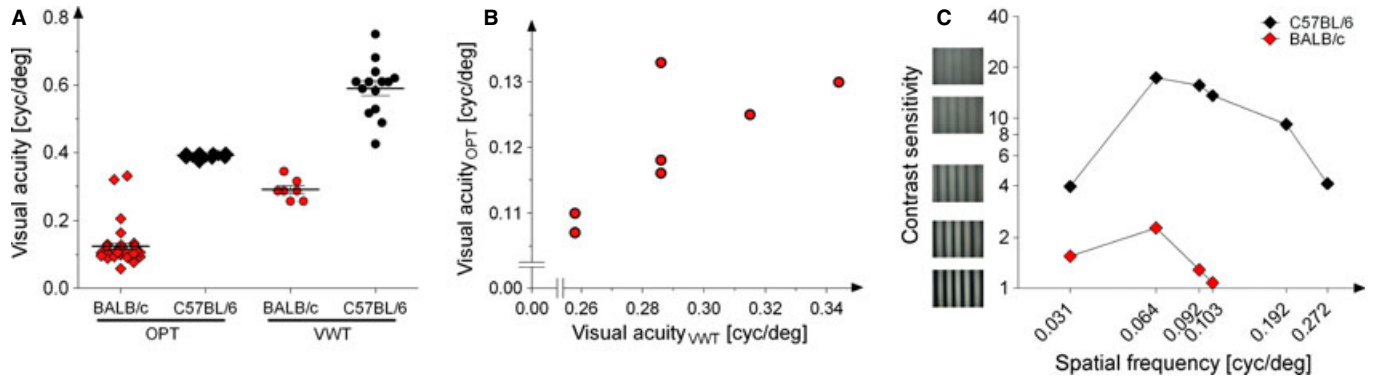

FIG. 3. Behaviourally determined visual performance of BALB/c and C57BL/6 mice. (A) Visual acuity was measured with both the virtual-reality optomotor setup (OPT) and the VWT. In both tests, the visual acuity of BALB/c mice was approximately 0.27–0.28 cyc/deg lower than that of C57BL/6 mice – the average acuity of BALB/c mice was 0.12 cyc/deg (OPT) and 0.3 cyc/deg (VWT), and the average acuity of C57BL/6 mice was 0.39 cyc/deg (OPT) and 0.59 cyc/deg (VWT). (B) In BALB/c mice, values measured in the two tasks were significantly correlated. (C) Contrast sensitivity measured at six different spatial frequencies in the OPT test. Sensitivity peaked at 0.64 cyc/deg in both strains. Contrast sensitivity was significantly lower in BALB/c than in C57BL/6 mice. A contrast sensitivity of 1 corresponds to ~100% contrast, and a contrast sensitivity of 2 corresponds to 50% contrast (see inset gratings). Error bars are included, but are too small to be visible. Note that BALB/c mice needed between three-fold and 12-fold higher contrast to elicit the optomotor response.

in the direction of the moving grating, as described previously (Prusky *et al.*, 2004; Lehmann & Löwel, 2008). Because the tracking response is triggered by stimuli moving in the temporo-nasal direction in pigmented mice, we next checked whether the wiring of the reflex was normal in this respect. To this end, we temporarily closed the right eye in a subset of five BALB/c mice, and analysed the optomotor response elicited by stimulation of the left eye only. In all five mice, the reflex was elicited only by gratings moving in the temporo-nasal direction, and thresholds were not different from those measured with both eyes open ($P > 0.05$, paired *t*-test).

Contrast sensitivity was measured at six different spatial frequencies (between 0.031 and 0.272 cyc/deg; Fig. 3C). In BALB/c and C57BL/6 mice, contrast sensitivity peaked at a spatial frequency of 0.064 cyc/deg, as described previously for C57BL/6 mice (Prusky *et al.*, 2004). However, in BALB/c mice, values were significantly lower than in the pigmented mice ($P < 0.001$, $F_{1,44} = 1383.44$, two-way ANOVA with repeated measures). Whereas pigmented mice tracked the moving gratings up to a contrast of only 5.8%, corresponding to a contrast sensitivity of 17.4 ± 0.3, at 0.064 cyc/deg ($n = 26$), BALB/c mice needed a contrast of 45% (corresponding to a contrast sensitivity of 2.2 ± 0.1, $n = 20$; Fig. 3C) for a reliable optomotor response. Contrast sensitivities of both genotypes at all spatial frequencies are listed in Table 1.

VWT

In the VWT, the animals have to learn to differentiate between two different visual stimuli, in our case between a vertical grating and equiluminant grey. During both training and testing in the VWT, BALB/c mice were slower than C57BL/6 mice. It turned out that this was attributable to both slower learning and lower swimming speed. In order to finish the training phase, i.e. to reach at least 90% correct trials in a block of 10 runs, BALB/c mice needed, on average, 148 ± 20 trials, as compared with 97 ± 3 trials for C57BL/6 mice ($P < 0.05$, *t*-test). Thus, training took 16 ± 2 days for BALB/c mice and 5 ± 0.3 days for C57BL/6 mice ($P < 0.01$, *t*-test). It should be mentioned that we trained all mice exclusively by operant conditioning, i.e. without shaping, and did not start testing until the 90% criterion was reached, whereas, in a previous study (Wong & Brown, 2006), animals were shaped during only 12 trials to learn the task. Concerning speed, the median latency to reach the platform in correct trials during the testing phase was 23.9 ± 2.5 s for BALB/c mice and 9.3 ± 1.7 s for C57BL/6 mice ($P < 0.001$, *t*-test). Furthermore, to accommodate the rapid fatigue of the BALB/c mice, we reduced the number of trials in a testing session from 10–15 to five.

In the VWT, the visual acuity in BALB/c mice was 0.30 ± 0.01 cyc/deg ($n = 7$) and thus significantly lower than in C57BL/6 mice (0.59 ± 0.02 cyc/deg, $n = 14$, $P < 0.001$, *t*-test; Fig. 3A). As the visual acuity values of BALB/c mice in the virtual optomotory system were determined by 'reverse' tracking, we also analysed whether the values obtained in both behavioural paradigms were correlated. We found that visual acuity values of the seven individual BALB/c mice that were tested in both paradigms were, indeed, correlated ($r = 0.76$, $P = 0.048$; Fig. 3B). In both strains, visual acuity as determined by the VWT was, on average, about 0.2 cyc/deg higher than in the optomotor setup, as previously also described for mice lacking the presynaptic active zone protein Bassoon (Goetze *et al.*, 2010).

TABLE 1. Contrast sensitivity at all measured spatial frequencies (mean ± standard error of the mean) of BALB/c and C57BL/6 mice; both absolute contrast and percentage values (in parentheses – lowest contrast eliciting an optomotor response) are shown

Cycles/degree	BALB/c	C57BL/6
0.031	1.5 ± 0.07 (66.4 ± 2.8)	4.0 ± 0.06 (25.5 ± 0.4)
0.064	2.2 ± 0.10 (45.3 ± 2.3)	17.4 ± 0.3 (5.8 ± 0.1)
0.092	1.3 ± 0.06 (79.7 ± 3.3)	15.7 ± 0.38 (6.5 ± 0.2)
0.103	1.1 ± 0.02 (93.5 ± 1.6)	13.6 ± 0.40 (7.6 ± 0.3)
0.192	–	9.2 ± 0.28 (11.2 ± 0.4)
0.272	–	4.1 ± 0.08 (24.7 ± 0.5)

Visual cortical activity maps in BALB/c mice

To analyse activity in the visual cortex in reponse to stimulation of the ipsilateral and contralateral eyes in BALB/c mice, we used optical imaging of intrinsic signals (Lehmann & Löwel, 2008). We visualized both elevation maps after visual stimulation with moving horizontal bars and azimuth maps after stimulation with moving vertical bars. Both the magnitude of the cortical responses and the retinotopic organization of the activity maps were compared in BALB/c and C57BL/6 mice.

Contralateral eye maps were normal in BALB/c mice

To study the cortical representation of the contralateral visual field in the left visual cortex, we restricted visual stimuli to the right visual field (Fig. 4). The average magnitude of the cortical responses was not significantly different between the two strains for either elevation or azimuth maps ($P > 0.5$, *t*-test). After visual stimulation of the contralateral eye, the signal amplitudes in elevation maps (Fig. 4A) were $(2.38 \pm 0.13) \times 10^{-4}$ in C57BL/6 mice ($n = 9$) and $(2.54 \pm 0.26) \times 10^{-4}$ in BALB/c mice ($n = 11$), and those in azimuth maps were $(2.07 \pm 0.12) \times 10^{-4}$ in C57BL/6 mice and $(2.07 \pm 0.25) \times 10^{-4}$ in BALB/c mice (Fig. 4B). In addition, visual cortical maps showed clear and apparently well-organized retinotopy in

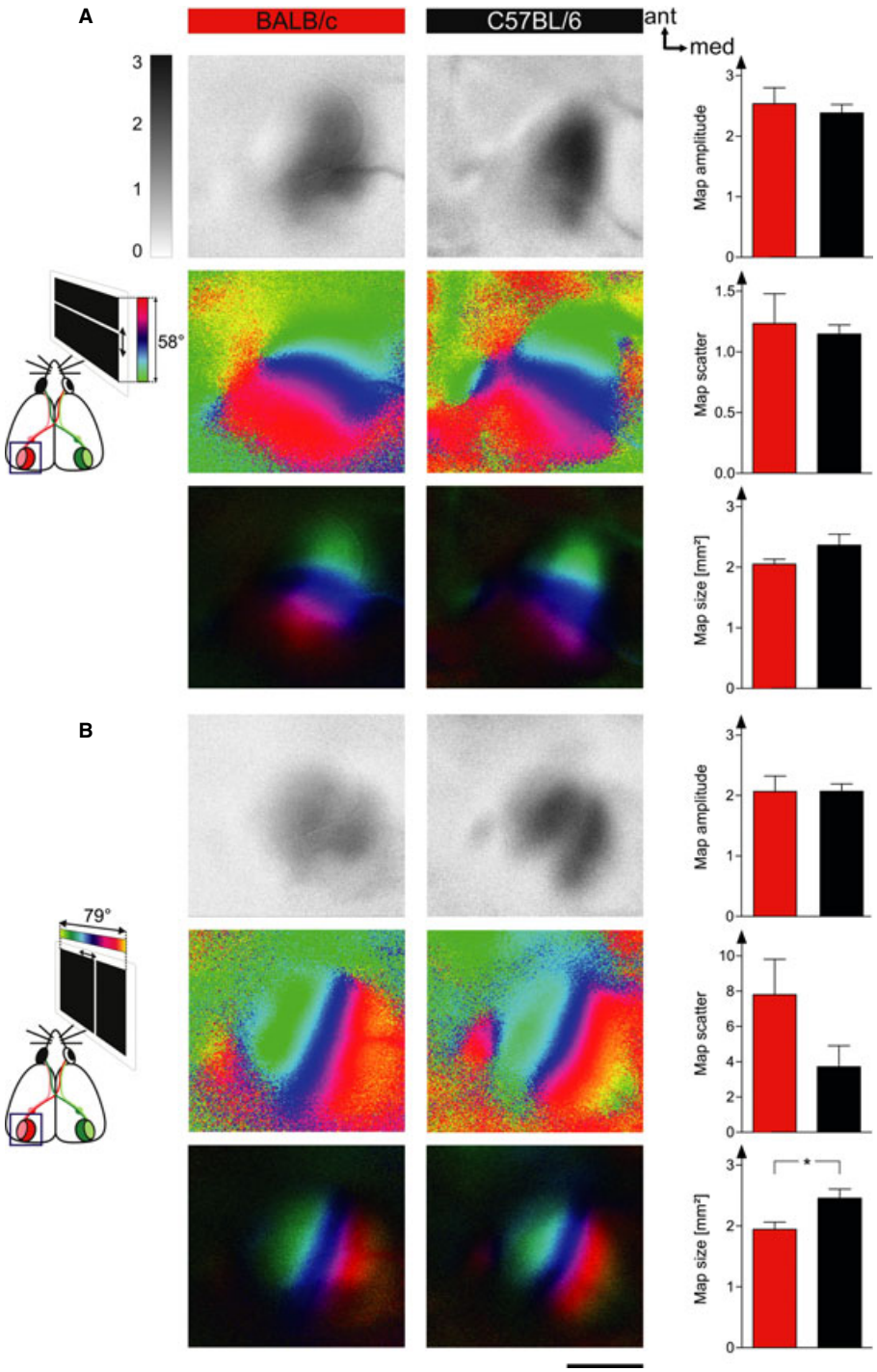

FIG. 4. Optically imaged visual cortical maps and their quantification in C57BL/6 and BALB/c mice. Visual cortical maps were similar in BALB/c and C57BL/6 mice. Both elevation (A) and azimuth (B) maps resulting from visual stimulation of the mice with moving horizontal bars (A) or vertical bars (B) are shown. Greyscale coded response magnitude maps (top), colour-coded phase maps (centre) and polar maps of retinotopy (below) are shown, together with their quantification (right column). The magnitude of the optical responses is expressed as fractional change in reflection $\times 10^{-4}$ – the greyscale bar at the top left applies to all amplitude maps. Retinotopic maps are colour-coded according to the schemes on the left side. Note that visual cortical maps of BALB/c mice had both response amplitude and retinotopy similar to those of visual cortical maps of C57BL/6 mice. The scale bar is 1 mm, and applies to all panels showing maps. $^*P < 0.05$

both strains – map scatters of elevation maps were 1.23 ± 0.24 in BALB/c mice and 1.15 ± 0.07 in C57BL/6 mice ($P > 0.5$, *t*-test). The map scatter of azimuth maps was 7.80 ± 2.0 in BALB/c mice, and thus higher than the 3.71 ± 1.19 in C57BL/6-mice. This difference was, however, not significant ($P > 0.1$, *t*-test). The size of elevation maps in BALB/c mice was 2.05 ± 0.08 mm^2, and thus not significantly different from that in C57BL/6 mice (2.36 ± 0.18 mm^2, $P = 0.087$, *t*-test). In contrast, azimuth maps in BALB/c mice covered 1.95 ± 0.12 mm^2 ($n = 11$), and were thus slightly, but significantly, smaller ($P < 0.05$, *t*-test) than those in C57BL/6 mice (2.45 ± 0.15 mm^2, $n = 9$; Fig. 4B).

Higher contralateral dominance in the visual cortex of BALB/c mice

Next, we restricted the stimulus to the binocular visual field of the recorded hemisphere to compare activity maps induced by stimulation of both the ipsilateral and contralateral eyes in the same region of the visual cortex. It turned out that reproducible ipsilateral eye maps could only be detected in nine BALB/c mice, whereas maps were at noise level in another 11 mice. These mice were therefore not included in the present quantification. In mice of both strains, visual stimulation of the contralateral eye induced visual cortical activity maps that were always darker than after stimulation of the ipsilateral eye, reflecting the dominance of the contralateral eye in the binocular region of the visual cortex (Fig. 5A and B) – the maximal activity amplitudes for contralateral eye stimulation were (2.3 ± 0.20) × 10^{-4} in BALB/c mice ($n = 9$) and (1.8 ± 0.09) × 10^{-4} in C57BL/6 mice ($n = 10$), and those for ipsilateral eye stimulation were (1.09 ± 0.14) × 10^{-4} in BALB/c mice and (1.2 ± 0.07) × 10^{-4} in C57BL/6 mice (Fig. 5D). Contralateral eye dominance was significantly stronger in BALB/c mice than in C57BL/6 mice: (i) quantification revealed that the ODI in BALB/c mice was, on average, 0.36 ± 0.03, and thus significantly

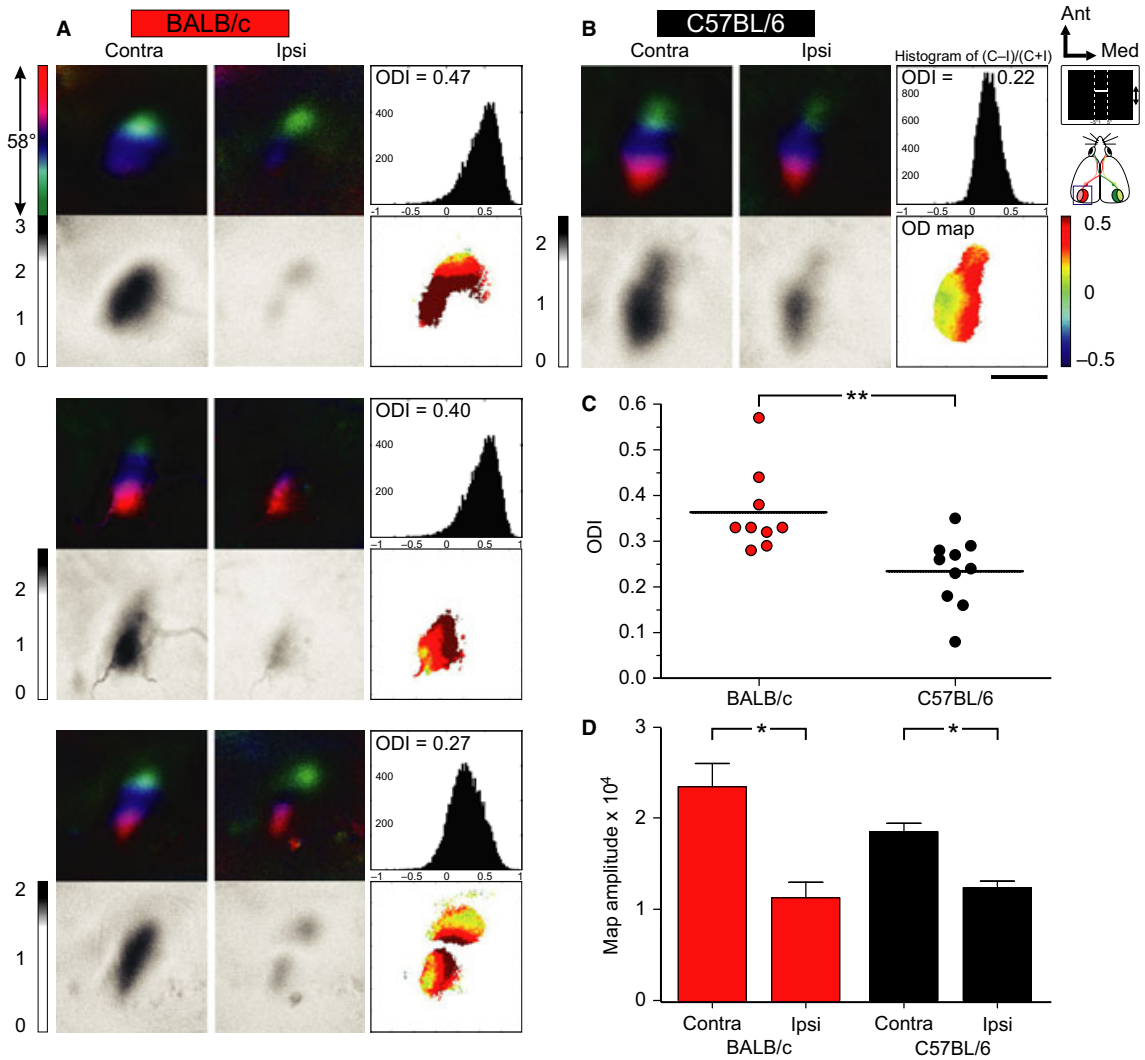

FIG. 5. Comparison of ipsilateral and contralateral eye maps in the visual cortex of BALB/c and C57BL/6 mice. BALB/c maps showed significantly higher contralateral eye dominance than C57BL/6 maps. Representative polar (top) and amplitude maps (below) induced by visual stimulation of the right binocular visual field (see inset at top right) through the contralateral and ipsilateral eyes of three BALB/c mice (A) and one C57BL/6 mouse (B). The elevation in polar maps is colour-coded according to the colour scheme on the left. For each experiment, the histogram of ocular dominance scores (top right), the average ODI (number in the histogram) and the corresponding two-dimensional ocular dominance maps (bottom right) are included (ODI values are colour-coded – blue, negative values; red, positive values). Note that, in both strains, the binocular visual cortex was dominated by input from the contralateral eye, as illustrated by histogram peaks biased to the right from zero and by warm colours in the ocular dominance maps. However, in BALB/c mice, this contralateral dominance was more pronounced than in C57BL/6 mice – the ocular dominance map contained more deep red, and the mean ODI was higher. Note that, in 11 of 20 animals, no maps could be recorded by ipsilateral eye stimulation. (C) Average ODIs are plotted for both strains. Each symbol represents the ODI of an individual mouse, and means are marked by thick horizontal lines. (D) Magnitude of both ipsilateral and contralateral eye maps in both strains. *$P < 0.05$; **$P < 0.01$.

higher than in C57BL/6 mice (0.23 ± 0.02, $P < 0.01$, *t*-test; Fig. 5C); and (ii) two-dimensional ocular dominance maps showed warmer colours (Fig. 5A and B).

Modified ipsilateral eye representation in BALB/c mice

When inspecting the layout of the ipsilateral eye maps, we had the qualitative impression of a 'waist' in the activity maps – regions representing the visual field slightly above the horizontal meridian, i.e. those represented by blue to blue–green colours, were often scarcely represented in BALB/c mice, whereas the lowest stimulated regions of the visual field, represented by green on the maps, were more conspicuous than in maps acquired from C57BL/6 mice (compare Figs 5A and B, and 6C and G). In contrast, activity maps from C57BL/6 mice almost always had an oval shape, with the strongest activity in the centre (Fig. 5B).

To quantify the impression that ipsilateral eye maps of BALB/c and C57BL/6 mice were different in topographic layout, we calculated the map 'volume', i.e. area multiplied by amplitude, in bins of 2° elevation, as a percentage of the total map volume (see Materials and methods). For C57BL/6 mice, this analysis resulted in bell-shaped curves with a single peak for both contralateral and ipsilateral eye stimulation (Fig. 6F and H). Stimulation in the lower part of the visual field appeared to activate the cortex more through the

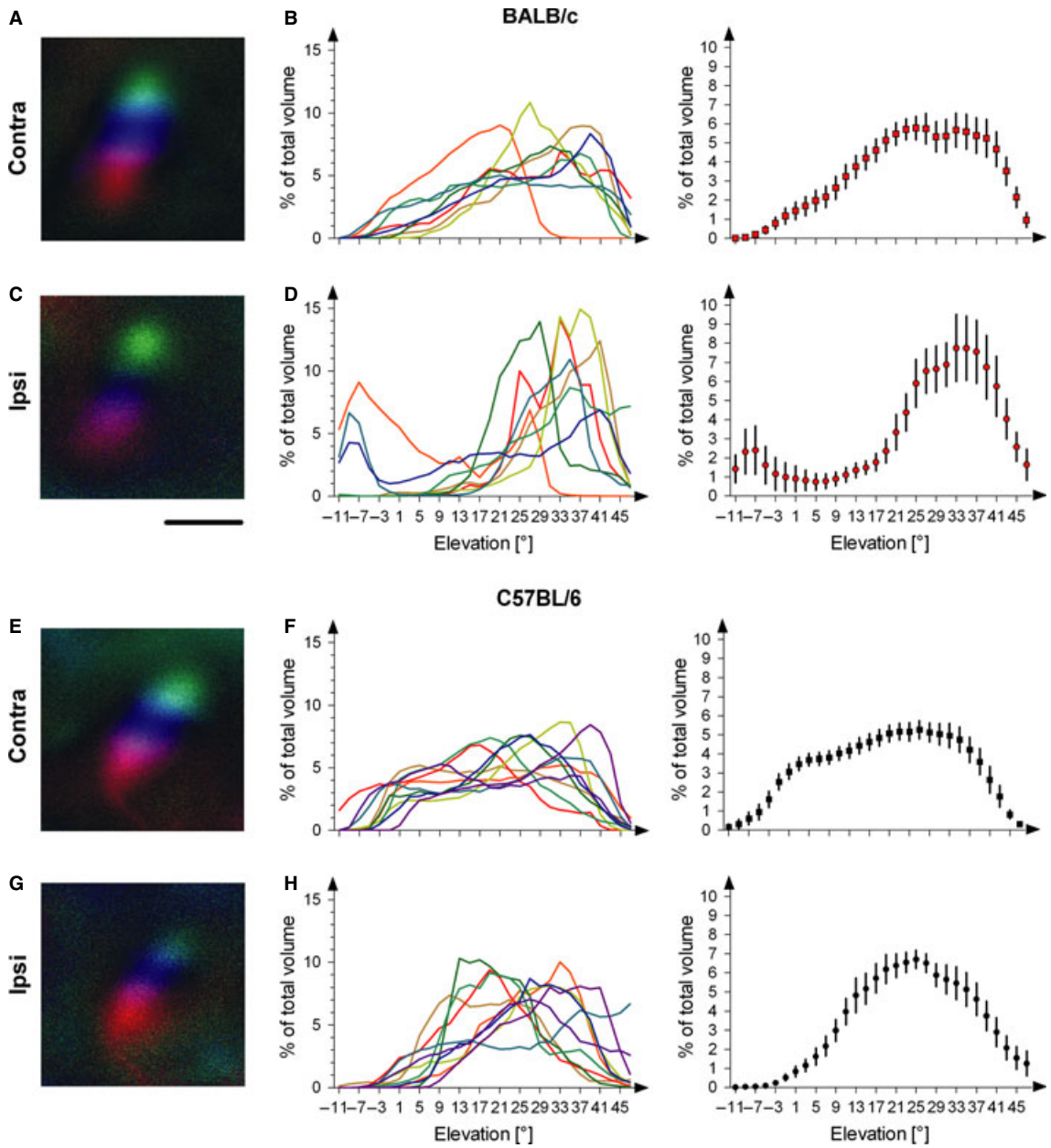

FIG. 6. Topography of binocular visual field maps of BALB/c and C57BL/6 mice. (A, C, E, and G) Representative maps of the binocular visual field elicited by stimulation of the contralateral and ipsilateral eyes of BALB/c mice (A and C) and C57BL/6 mice (E and G) are shown. Note that activity coded by blue to blue–green shading in the C57BL/6 ipsilateral eye maps was lacking in the BALB/c maps. Scale bar – 1 mm. (B, D, F, and H) For quantification, the activity of map pixels was summed up in bins of 2° elevation, and expressed as percentage of whole map activity ('volume'). Traces for individual mice (central column) and averages (right column) are shown for both contralateral and ipsilateral eye maps in BALB/c mice (B and D) and C57BL/6 mice (F and H). Note the conspicuous dip in BALB/c ipsilateral eye maps at approximately 5°–9° elevation.

contralateral than the ipsilateral eye. Statistical analysis confirmed this impression for the range of −1° to 5° (Fig. 6B; $P < 0.05$ at −1° and 5°, $P < 0.01$ at 1° and 3°, Bonferroni-corrected *t*-tests).

The topography of retinotopic maps from BALB/c mice was markedly different. Whereas maps acquired by stimulation of the contralateral eye in the binocular field were statistically indistinguishable from the corresponding maps from C57BL/6 mice (Fig. 7C), in spite of an apparently weaker representation of the lower visual field reminiscent of C57BL/6 ipsilateral eye maps, stimulation of the ipsilateral eye resulted in maps that had a more narrow main peak that was occasionally accompanied by a second, smaller peak (Fig. 5D). In BALB/c mice, the strongest activation was at approximately 33° elevation, declining to both sides, with the lowest activation at approximately 5° elevation. If present, the second smaller 'peak' was at approximately −7° elevation, an area that was left almost uncovered in C57BL/6 mice, and by the contralateral eye of BALB/c mice (Fig. 7A and D). Statistical analyses confirmed that, in BALB/c ipsilateral eye maps, the area of 15° to 19° elevation was significantly less represented than in C57BL/6 eye maps (Fig. 7D; $P < 0.05$, Bonferroni-corrected *t*-tests). This area was also less represented by the ipsilateral than by the contralateral eye in BALB/c mice (Fig. 7A), but this difference was not significant ($P = 0.078$ and $P = 0.065$, respectively, Bonferroni-corrected *t*-tests). Similarly, the second, minor peak of the BALB/c ipsilateral eye maps was also not statistically different from that of the BALB/c contralateral or C57BL/6 ipsilateral eye maps.

Discussion

To our knowledge, this is the first study in which the visual capabilities of BALB/c mice have been investigated in detail. BALB/c mice have low visual acuity in both the virtual-reality optomotor system (0.12 cyc/deg) and in the VWT (0.3 cyc/deg). Visual acuity values were thus ∼ 0.28 cyc/deg below those measured in C57BL/6 mice (optometry, 0.39 cyc/deg; VWT, 0.58 cyc/deg). Interestingly, this is about the same acuity difference as measured previously by optometry in albino and pigmented rats (0.25 cyc/deg vs. 0.53 cyc/deg) (Douglas *et al.*, 2005). Previous attempts to determine visual acuity in BALB/c mice by the optokinetic tracking reflex had failed, probably because of the use of the less sophisticated optokinetic drum (Puk *et al.*, 2008). Whereas an optokinetic nystagmus could not be elicited in drum measurements in albino rats (Precht & Cazin, 1979), the recently developed virtual-reality optomotor system allows determination of visual acuity thresholds on the basis of minute but visible tracking in albino rodents (Douglas *et al.*, 2005). Using the same virtual-reality optomotor system, we observed reflexive head movements of very quick onset and rapid decay that were, however, in a direction opposite to the moving gratings in BALB/c mice. Such an 'inverted' optokinetic nystagmus has been described before in albino rabbits and rats, as well as in hypopigmented mutant pearl and beige mice (Collewijn *et al.*, 1978; Balkema *et al.*, 1984; Sirkin *et al.*, 1985; Pak *et al.*, 1987). This may be an analogue of the horizontal peduncular nystagmus in human albinos, as failure of the feedback stabilization of the retinal image would be expected to lead to a build-up of oscillations. The anatomical basis for this inverted reflex is not clear, but, in several albino rodent species, it has been shown that the retinopretectal projection mediating this reflex completely crosses, whereas uncrossed fibres are present in pigmented animals (Lund, 1965; Giolli & Creel, 1973; Collewijn *et al.*, 1978; Klooster *et al.*, 1983).

Thus, the low visual acuity of BALB/c mice measured in the virtual-reality optomotor system could reflect a miswiring of the subcortical pathways mediating the optokinetic reflex (Douglas *et al.*,

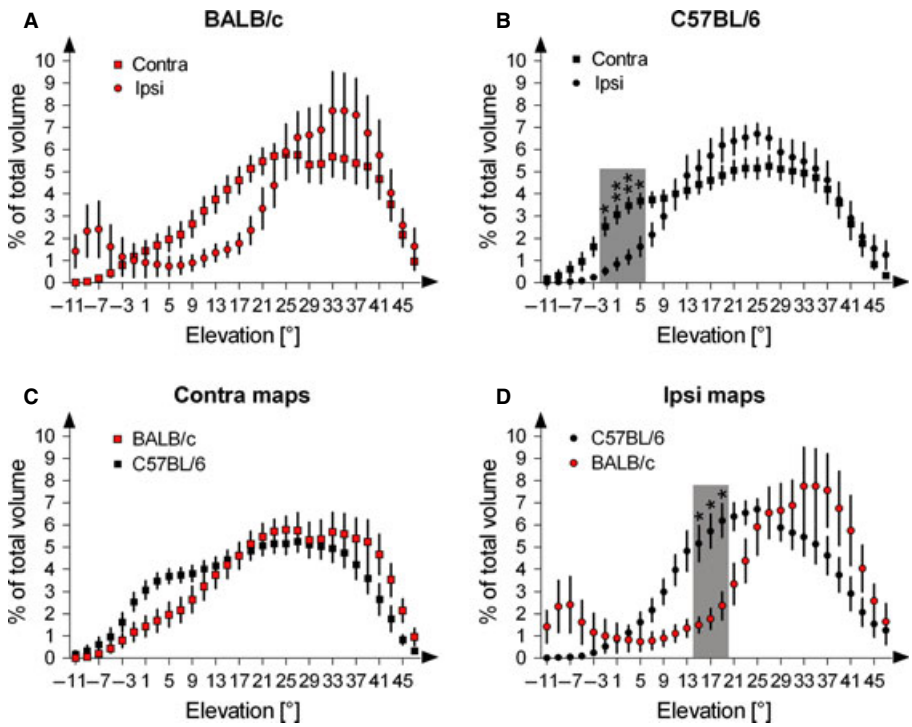

FIG. 7. The topography of ipsilateral retinotopic maps is different between C57BL/6 and BALB/c mice. (A) In BALB/c mice, a gap in ipsilateral visual field representation was found in the visual field between approximately 1° and 19° elevation. (B) In C57BL/6 mice, the lower visual field was more strongly represented by the contralateral than the ipsilateral eye. (C) Contralateral eye maps were similar in the two strains, although the central visual field appeared less represented in BALB/c than in C57BL/6 mice. (D) In ipsilateral eye maps, in contrast, representation of the area above the horizon was significantly reduced in BALB/c as compared with C57BL/6 mice. *$P < 0.05$; **$P < 0.01$. All asterisks are stacked vertically.

2005; Cahill & Nathans, 2008), rather than the optimal spatial resolution of the visual system. We therefore additionally tested visual acuity in the VWT, a visual discrimination task that is known to depend on the visual cortex (Prusky *et al.*, 2000; Prusky & Douglas, 2004; Douglas *et al.*, 2005). As was observed previously (Wong & Brown, 2006), BALB/c animals took a long time to learn the task and to be tested. This may, in part, be attributable to the motor, emotional and cognitive impairments observed in this strain (Nowakowski, 1984; Lassalle *et al.*, 1994; Klapdor & van der Staay, 1996; McFadyen *et al.*, 2003; Wong & Brown, 2006). Nevertheless, by adapting the testing conditions to the specific requirements of this strain, we were able to measure a visual acuity of 0.3 cyc/deg, which, as in C57BL/6 mice, is $\sim$ 0.2 cyc/deg above the value obtained in the virtual-reality optomotor system, but only about half that for the pigmented strain. A similar relationship has previously been observed in rats – in the VWT, three albino rat strains achieved half the spatial resolution of pigmented rats (Prusky *et al.*, 2002).

The reasons for this poor visual performance in albino rodents are not immediately clear. Apart from the lack of pigmentation in the pigment epithelium and the reduced thickness of the entire retina, layering of the retina appeared to be regular in our stainings and OCT measurements. At 1 month of age, there is no difference in rod density between C57BL/6 and BALB/c mice, but the age-related loss of rods in both strains is much more pronounced in the albinos at 17 months (Gresh *et al.*, 2003). Additionally, we observed a hitherto undescribed abnormality in the macrostructure of the BALB/c retina, which appeared wavy and had varying thicknesses of layers. This may result from anomalies in retinal development, with imprecisely orchestrated birth and elimination of cells, as documented for albino rats (Ilia & Jeffery, 2000). Structural irregularities in the retina could then lead to alterations in neuronal information processing. Indeed, a prolonged b-wave, originating from retinal interneuronal firing, of lower amplitude in the electroretinogram of adult BALB/c mice than in that of C57BL/6 mice has been observed (Gresh *et al.*, 2003). It is thus possible that the reasons for the poor visual capabilities of BALB/c mice may reside inside the retina.

To check for cortical involvement in the peculiarities of visually guided behaviour observed in BALB/c mice, we investigated visual cortical activity maps recorded by optical imaging of intrinsic signals. In general, the cortical representation of the visual world appeared to be rather normal in BALB/c mice. Activity maps induced by visual stimulation of the contralateral eye had similar magnitude and quality as for C57BL/6 mice. This is in contrast to a previous report of lower total cortical responses in BALB/c mice as measured by optical imaging (Heimel *et al.*, 2007). The difference may be attributable to either different methods of stimulation and data acquisition – episodic vs. periodic imaging – or to the fact that Heimel *et al.* stimulated both eyes simultaneously, such that the weak ipsilateral signal may have interfered with the cortical maps in BALB/c mice. The finding that cortical maps of the contralateral visual field in BALB/c mice were normal in spite of severe impairments in visual capabilities is totally in line with our recent observations in Bassoon mutant mice, which also displayed normal visual cortical activity maps, notwithstanding a pronounced photoreceptor synaptopathy and a strong reduction in the electroretinogram b-wave (Dick *et al.*, 2003; Goetze *et al.*, 2010). As the spatial frequency of the stimulus for optical imaging is below the behaviourally measured discrimination threshold, the recorded maps principally reflect the retinotopic organization of the visual cortex, and activity maps are not visibly influenced even in animals with lesioned or sick retinas (Krempler *et al.*, 2011; Goetze *et al.*, 2010).

Although activity maps of the contralateral eye appeared rather normal, we observed a peculiar shape of the ipsilateral eye maps in V1, with a 'waist' resulting in a scarce representation of a visual field region at approximately 17° elevation. The origin of this unusual map topography is unclear. In albino C57BL/6 mice, lower numbers and proportions of ipsilaterally projecting retinal ganglion cells than in pigmented animals have been documented (Dräger & Olsen, 1980), and, in the radial direction (corresponding to azimuth in the binocular, temporal part of the retina), their density dropped along a gradient from the retinal edge towards the inner margin of the ipsilateral crescent, whereas, in pigmented animals, it remained high in the outer two-thirds of the crescent before declining (Dräger & Olsen, 1980). However, no abnormal distribution pattern in the angular direction was described. Nevertheless, the finding that the visual field is weakly mapped in an area along the vertical meridian calls to mind the fact that a fovea or visual streak is lacking in albino animals of species that possess such a structure (Wilson *et al.*, 1988; Donatien *et al.*, 2002). Mice have little or no visual streak to start with (Salinas-Navarro *et al.*, 2009), but it is conceivable that the same mechanisms that produce the absence of a visual streak in higher mammals are active in albino mice, thus creating what might be called an 'inverted visual streak'. Birthdating studies suggest that the lack of 3,4-dihydroxy-phenylalanine in the albino retina leads to increased production of both photoreceptor and ganglion cells (Ilia & Jeffery, 2000; Rachel *et al.*, 2002). This overproduction could then result in disturbances in apoptosis and cell fate decision, and could thus create the albino retinal phenotype; it might also explain the varying thickness of retinal layers observed in our stainings.

In summary, the visual system of BALB/c mice exhibits a number of features that are characteristic for albinos of all mammalian species – low visual acuity, disturbed horizontal optokinetic response, and a weak and modified cortical representation of the ipsilateral eye that may impair stereopsis. These visual impairments need to be taken into account when BALB/c mice are subjected to behavioural tests that rely on visual information, or when they are suggested as a model system to study neuropsychological disorders.

Supporting Information

Additional supporting information can be found in the online version of this article:

Movie S1. A BALB/c mouse is tested in the virtual-reality optomotor system. The moving vertical gratings induce an optomotor response (head movements) against the direction of the rotating gratings.

Please note: As a service to our authors and readers, this journal provides supporting information supplied by the authors. Such materials are peer-reviewed and may be re-organized for online delivery, but are not copy-edited or typeset by Wiley-Blackwell. Technical support issues arising from supporting information (other than missing files) should be addressed to the authors.

Acknowledgements

We wish to thank Bianka Götze and Katja Krempler for help with some of the experiments. Thanks are also due to Elke Woker for excellent animal care. Support of the Bundesministerium für Bildung und Forschung (BMBF) (01GQ0810 to S. Löwel, and 01KW9923 and 01GS0850 to J. Graw) is gratefully acknowledged. This study was additionally funded by a DAAD grant to N. Yeritsyan.

Abbreviations

OCT, optical coherence tomography; ODI, ocular dominance index; P, postnatal day; VWT, visual water task.

References

Balkema, G.W., Mangini, N.J., Pinto, L.H. & Vanable, J.W. Jr (1984) Visually evoked eye movements in mouse mutants and inbred strains. A screening report. *Invest. Ophthalmol. Vis. Sci.*, **25**, 795–800.

Brodkin, E.S. (2007) BALB/c mice: low sociability and other phenotypes that may be relevant to autism. *Behav. Brain Res.*, **176**, 53–65.

Cahill, H. & Nathans, J. (2008) The optokinetic reflex as a tool for quantitative analyses of nervous system function in mice: application to genetic and drug-induced variation. *PLoS ONE*, **3**, e2055.

Cang, J., Kalatsky, V.A., Löwel, S. & Stryker, M.P. (2005a) Optical imaging of the intrinsic signal as a measure of cortical plasticity in the mouse. *Vis. Neurosci.*, **22**, 685–691.

Cang, J., Kaneko, M., Yamada, J., Woods, G., Stryker, M.P. & Feldheim, D.A. (2005b) Ephrin-as guide the formation of functional maps in the visual cortex. *Neuron*, **48**, 577–589.

Collewijn, H., Winterson, B.J. & Dubois, M.F. (1978) Optokinetic eye movements in albino rabbits: inversion in anterior visual field. *Science*, **199**, 1351–1353.

Dick, O., tom Dieck, S., Altrock, W.D., Ammermuller, J., Weiler, R., Garner, C.C., Gundelfinger, E.D. & Brandstatter, J.H. (2003) The presynaptic active zone protein bassoon is essential for photoreceptor ribbon synapse formation in the retina. *Neuron*, **37**, 775–786.

Donatien, P., Aigner, B. & Jeffery, G. (2002) Variations in cell density in the ganglion cell layer of the retina as a function of ocular pigmentation. *Eur. J. Neurosci.*, **15**, 1597–1602.

Douglas, R.M., Alam, N.M., Silver, B.D., McGill, T.J., Tschetter, W.W. & Prusky, G.T. (2005) Independent visual threshold measurements in the two eyes of freely moving rats and mice using a virtual-reality optokinetic system. *Vis. Neurosci.*, **22**, 677–684.

Dräger, U.C. (1974) Autoradiography of tritiated proline and fucose transported transneuronally from the eye to the visual cortex in pigmented and albino mice. *Brain Res.*, **82**, 284–292.

Dräger, U.C. & Olsen, J.F. (1980) Origins of crossed and uncrossed retinal projections in pigmented and albino mice. *J. Comp. Neurol.*, **191**, 383–412.

Fischer, M.D., Huber, G., Beck, S.C., Tanimoto, N., Muehlfriedel, R., Fahl, E., Grimm, C., Wenzel, A., Reme, C.E., van de Pavert, S.A., Wijnholds, J., Pacal, M., Bremner, R. & Seeliger, M.W. (2009) Noninvasive, *in vivo* assessment of mouse retinal structure using optical coherence tomography. *PLoS ONE*, **4**, e7507.

Giolli, R.A. & Creel, D.J. (1973) The primary optic projections in pigmented and albino guinea pigs: an experimental degeneration study. *Brain Res.*, **55**, 25–39.

Goetze, B., Schmidt, K.F., Lehmann, K., Altrock, W.D., Gundelfinger, E.D. & Löwel, S. (2010) Vision and visual cortical maps in mice with a photoreceptor synaptopathy: reduced but robust visual capabilities in the absence of synaptic ribbons. *Neuroimage*, **49**, 1622–1631.

Gresh, J., Goletz, P.W., Crouch, R.K. & Rohrer, B. (2003) Structure–function analysis of rods and cones in juvenile, adult, and aged C57bl/6 and Balb/c mice. *Vis. Neurosci.*, **20**, 211–220.

Heimel, J.A., Hartman, R.J., Hermans, J.M. & Levelt, C.N. (2007) Screening mouse vision with intrinsic signal optical imaging. *Eur. J. Neurosci.*, **25**, 795–804.

Holthoff, K., Kovalchuk, Y., Yuste, R. & Konnerth, A. (2004) Single-shock LTD by local dendritic spikes in pyramidal neurons of mouse visual cortex. *J. Physiol.*, **560**, 27–36.

Ilia, M. & Jeffery, G. (2000) Retinal cell addition and rod production depend on early stages of ocular melanin synthesis. *J. Comp. Neurol.*, **420**, 437–444.

Kalatsky, V.A. & Stryker, M.P. (2003) New paradigm for optical imaging: temporally encoded maps of intrinsic signal. *Neuron*, **38**, 529–545.

Klapdor, K. & van der Staay, F.J. (1996) The Morris water-escape task in mice: strain differences and effects of intra-maze contrast and brightness. *Physiol. Behav.*, **60**, 1247–1254.

Klooster, J., van der Want, J.J. & Vrensen, G. (1983) Retinopretectal projections in albino and pigmented rabbits: an autoradiographic study. *Brain Res.*, **288**, 1–12.

Kohara, K., Yasuda, H., Huang, Y., Adachi, N., Sohya, K. & Tsumoto, T. (2007) A local reduction in cortical GABAergic synapses after a loss of endogenous brain-derived neurotrophic factor, as revealed by single-cell gene knock-out method. *J. Neurosci.*, **27**, 7234–7244.

Krempler, K., Schmeer, C.W., Isenmann, S., Witte, O.W. & Löwel, S. (2011) Simvastatin improves retinal ganglion cell survival and spatial vision after acute retinal ischemia/reperfusion in mice. *Invest Ophthalmol. Vis. Sci.*, **52**, 2606–2618.

Lassalle, J.M., Halley, H. & Roullet, P. (1994) Analysis of behavioral and hippocampal variation in congenic albino and pigmented BALB mice. *Behav. Genet.*, **24**, 161–169.

Lehmann, K. & Löwel, S. (2008) Age-dependent ocular dominance plasticity in adult mice. *PLoS ONE*, **3**, e3120.

Lepicard, E.M., Venault, P., Abourachid, A., Pelle, E., Chapouthier, G. & Gasc, J.P. (2006) Spatio-temporal analysis of locomotion in BALB/cByJ and C57BL/6J mice in different environmental conditions. *Behav. Brain Res.*, **167**, 365–372.

Lund, R.D. (1965) Uncrossed visual pathways of hooded and albino rats. *Science*, **149**, 1506–1507.

McFadyen, M.P., Kusek, G., Bolivar, V.J. & Flaherty, L. (2003) Differences among eight inbred strains of mice in motor ability and motor learning on a rotorod. *Genes Brain Behav.*, **2**, 214–219.

Moy, S.S., Nadler, J.J., Poe, M.D., Nonneman, R.J., Young, N.B., Koller, B.H., Crawley, J.N., Duncan, G.E. & Bodfish, J.W. (2008) Development of a mouse test for repetitive, restricted behaviors: relevance to autism. *Behav. Brain Res.*, **188**, 178–194.

Nowakowski, R.S. (1984) The mode of inheritance of a defect in lamination in the hippocampus of BALB/c mice. *J. Neurogenet.*, **1**, 249–258.

Pak, M.W., Giolli, R.A., Pinto, L.H., Mangini, N.J., Gregory, K.M. & Vanable, J.W. Jr (1987) Retinopretectal and accessory optic projections of normal mice and the OKN-defective mutant mice beige, beige-J, and pearl. *J. Comp. Neurol.*, **258**, 435–446.

Precht, W. & Cazin, L. (1979) Functional deficits in the optokinetic system of albino rats. *Exp. Brain Res.*, **37**, 183–186.

Prusky, G.T. & Douglas, R.M. (2004) Characterization of mouse cortical spatial vision. *Vision. Res.*, **44**, 3411–3418.

Prusky, G.T., Alam, N.M., Beekman, S. & Douglas, R.M. (2004) Rapid quantification of adult and developing mouse spatial vision using a virtual optomotor system. *Invest. Ophthalmol. Vis. Sci.*, **45**, 4611–4616.

Prusky, G.T., Harker, K.T., Douglas, R.M. & Whishaw, I.Q. (2002) Variation in visual acuity within pigmented, and between pigmented and albino rat strains. *Behav. Brain Res.*, **136**, 339–348.

Prusky, G.T., West, P.W. & Douglas, R.M. (2000) Behavioral assessment of visual acuity in mice and rats. *Vision. Res.*, **40**, 2201–2209.

Puk, O., Dalke, C., Hrabe de Angelis, M. & Graw, J. (2008) Variation of the response to the optokinetic drum among various strains of mice. *Front. Biosci.*, **13**, 6269–6275.

Rachel, R.A., Dolen, G., Hayes, N.L., Lu, A., Erskine, L., Nowakowski, R.S. & Mason, C.A. (2002) Spatiotemporal features of early neuronogenesis differ in wild-type and albino mouse retina. *J. Neurosci.*, **22**, 4249–4263.

Salinas-Navarro, M., Jimenez-Lopez, M., Valiente-Soriano, F.J., Alarcon-Martinez, L., Aviles-Trigueros, M., Mayor, S., Holmes, T., Lund, R.D., Villegas-Perez, M.P. & Vidal-Sanz, M. (2009) Retinal ganglion cell population in adult albino and pigmented mice: a computerized analysis of the entire population and its spatial distribution. *Vision. Res.*, **49**, 637–647.

Sankoorikal, G.M., Kaercher, K.A., Boon, C.J., Lee, J.K. & Brodkin, E.S. (2006) A mouse model system for genetic analysis of sociability: C57BL/6J versus BALB/cJ inbred mouse strains. *Biol. Psychiatry*, **59**, 415–423.

Sirkin, D.W., Hess, B.J. & Precht, W. (1985) Optokinetic nystagmus in albino rats depends on stimulus pattern. *Exp. Brain Res.*, **61**, 218–221.

Wilson, H.R., Mets, M.B., Nagy, S.E. & Kressel, A.B. (1988) Albino spatial vision as an instance of arrested visual development. *Vision. Res.*, **28**, 979–990.

Wong, A.A. & Brown, R.E. (2006) Visual detection, pattern discrimination and visual acuity in 14 strains of mice. *Genes Brain Behav.*, **5**, 389–403.